Shahmohammadi et al., *BioImpacts.* 2024;14(5):30193
doi: 10.34172/bi.2024.30193
https://bi.tbzmed.ac.ir/

Burn wound healing using adipose-derived mesenchymal stem cells and manganese nanoparticles in polycaprolactone/gelatin electrospun nanofibers in rats

Azin Shahmohammadi[1], Hadi Samadian[2], Saeed Heidari Keshel[1], Khodabakhsh Rashidi[3], Amir Kiani[4], Masoud Soleimani[1*], Farjam Goudarzi[4*]

[1]Department of Applied Cell Sciences and Tissue Engineering, School of Advanced Technologies in Medicine, Shahid Beheshti University of Medical Sciences, Tehran, Iran
[2]Research Center for Molecular Medicine, Hamadan University of Medical Sciences, Hamadan, Iran
[3]Research Center of Oils and Fats, Kermanshah University of Medical Sciences, Kermanshah, Iran
[4]Regenerative Medicine Research Center, Kermanshah University of Medical Sciences, Kermanshah, Iran

Article Info

Article Type:
Original Article

Article History:
Received: 10 Dec. 2023
Revised: 1 Jan. 2024
Accepted: 2 Jan. 2024
ePublished: 21 Jan. 2024

Keywords:
Adipose-derived mesenchymal stem cells, Manganese nanoparticles, Burn wound, Electrospun nanofibers, Polycaprolactone/gelatin, Stem cell therapy

Abstract

Introduction: Wound healing is a major therapeutic concern in regenerative medicine. The current study aimed to investigate the second-degree burn wound treatment in rats using rat adipose-derived stem cells (ADSCs) and manganese nanoparticles (MnO_2–NPs) in a polycaprolactone/gelatin electrospun nanofiber scaffold.

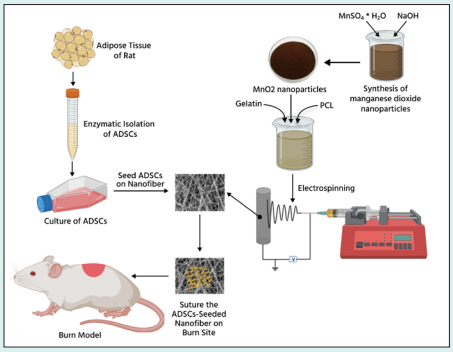

Methods: After the synthesis of nanoparticles and electrospinning of nanofibers, the SEM analysis, contact angle, mechanical strength, blood compatibility, porosity, swelling, biodegradability, cell viability, and adhesion assays were performed. According to the results, the PCL/Gel/5%MnO_2-NPs nanofiber (Mn-5%) was determined to be the most suitable scaffold. The ADSCs-seeded Mn-5% scaffolds were applied as a burn wound dressing. The wound closure rate, IL-1β, and IL-6 level, hydroxyproline, and glycosaminoglycans content were measured, and the hematoxylin and eosin, Masson's trichrome, and immunohistochemistry stainings were carried out.

Results: Based on the results, in Mn+S (ADSCs+PCL/Gel/5%MnO_2-NPs nanofiber) and N+S (ADSCs+PCL/Gel nanofiber) groups, the IL-6 and IL-1β levels were reduced, and the percentage of wound closure, glycosaminoglycans, and hydroxyproline content were increased compared to the control group (P<0.05). Also, the lowest amount of α-SMA was observed in these two groups, demonstrating stem cells' role in reducing α-SMA levels and thus preventing fibrosis. Moreover, the amount of α-SMA in the Mn+S group is lower than in the N+S group and, is closer to healthy skin. According to histology results, the best type of treatment was observed in the Mn+S group.

Conclusion: In conclusion, the ADSCs-seeded PCL/Gel/5%MnO_2-NPs scaffold demonstrated considerable therapeutic effects in burn wound healing.

Introduction

Skin plays an important part in many physiological functions, such as environmental protection, fluid balance, sensory input detection, metabolizing vitamin D, and self-healing.[1] Skin infections potentially delay recovery and increase patient morbidity and mortality.[2]

Healing a wound involves several steps, including hemostasis, inflammation, proliferation, and remodeling. Cell therapy has sparked much attention because of its application in skin tissue regeneration.[3] Cell therapy using autologous cells speeds up wound healing by decreasing the duration required for host cells to enter the damaged tissue and by promoting early skin regeneration.[4]

In tissue engineering, human adipose-derived mesenchymal stem cells (ADSCs) were discovered as a key cell source, due to their hypoimmunogenic characteristic,

*Corresponding authors: Masoud Soleimani, Email: soleimani.masoud@gmail.com; Farjam Goudarzi, Email: farjam.goudarzi@gmail.com

© 2024 The Author(s). This work is published by BioImpacts as an open access article distributed under the terms of the Creative Commons Attribution Non-Commercial License (http://creativecommons.org/licenses/by-nc/4.0/). Non-commercial uses of the work are permitted, provided the original work is properly cited.

ease of isolation, and broad proliferation capabilities.[5] It has also been demonstrated that ADSCs help during different stages of wound healing by releasing various anti-inflammatory cytokines and growth factors, stimulating the formation of new blood vessels and resurfacing with new epithelium, and balancing fibroblast characteristics and extracellular matrix (ECM) deposition.[6] Furthermore, studies have indicated that administering ADSCs decreases scarring, although the processes are not entirely understood.[7,8] ADSCs have become an important element in cell-based skin bioengineering due to their outstanding proliferation and differentiation capabilities.

Using stem cells with biomaterials is becoming very important in regenerative medicine.[9] A suitable tissue scaffold must exhibit good mechanical qualities and high biocompatibility for wound healing applications.[10]

The interconnected porous structure forms a significant portion of the electrospun nanofibrous mesh.[11,12] Electrospinning is successful in creating continuous polymer nanofibers with diameters ranging from micron to nanoscale and with great surface-to-volume ratio to provide better characteristics for wound treatment.[13]

Electrospun nanofibers have several benefits over standard dressings, including the capacity to simulate the native extracellular matrix, appropriate oxygen permeability, porosity, evaporation of water, and sustained discharge of active compounds.[14]

Many electrospun meshes have been employed for wound regeneration, notably polycaprolactone (PCL)-based mats, which have FDA approval and have high mechanical qualities.[15,16]

PCL (a synthetic polymer) has attracted many considerations due to its interesting mechanical characteristics and cytocompatibility. However, the hydrophobic nature of PCL restricts its use for wound dressing. For better hydrophilic characteristics, biocompatibility, and mechanical integrity, PCL has been combined with gelatin methacryloyl (GelMA).[17]

Gelatin is one of the most commonly used natural polymers and is produced by partially hydrolyzing the original collagen. Due to its lower molecular weight than collagen, gelatin is more easily and steadily electrospun. Additionally, it has a lot of integrin binding sites for cell motility, adhesion, and differentiation.[18] According to Seokwon's study,[19] combining gelatin and PCL is an effective way to overcome their weaknesses. It has also shown promises for use in the building of various tissues, including skin,[20] nerves,[21] muscles,[22] and dental works.[23]

It has been revealed that manganese levels rise within scars, emphasizing the significance of antioxidant function in the process of wound treatment (including mucopolysaccharide and glycoprotein formation, as well as mitochondrial antioxidant defense via manganese superoxide dismutase (Mn-SOD).[24] Manganese improves wound healing by activating matrix metalloproteinase-2/9.[25] According to the findings of an experiment, the synthetic MnNPs@ZC (green synthesized manganese nanoparticles using *Ziziphora clinopodioides* Lam leaves) exhibited antifungal, antibacterial (gram-negative and positive bacteria), antioxidant, non-cytotoxicity, and skin wound healing activities. These manganese nanoparticles can be employed in humans to treat skin and infectious disorders if confirmed in clinical trials.[26]

The purpose of the present study was to use the rat ADSCs and manganese nanoparticles in PCL/Gel electrospun nanofiber to treat second-degree burn wounds in rats. This new combination (ADSCs-seeded PCL/Gel/MnO2-NPs nanofiber) was investigated for the first time in this study and the obtained results confirmed the effectiveness of this treatment strategy.

Materials and Methods

Synthesis of manganese dioxide nanoparticles

The manganese dioxide nanoparticles (MnO2-NPs) were synthesized using the co-precipitation method according to the published paper by Cherian et al.[27] Aqueous solutions of 1 M manganese sulfate (manganese (II) sulfate monohydrate) and 2 M sodium hydroxide were used as reactants.100 mL of 2 M NaOH solution (freshly prepared) was incorporated dropwise to 100 mL of 1 M manganese sulfate solution. To precipitate the nanoparticles, the obtained solution was continuously stirred at 60 °C for 2 hours. Following that, the precipitate was separated using centrifugation (4000 rpm, 10 minutes), washed with deionized water, and then finally dried at room temperature.

Polycaprolactone/gelatin nanofiber

To make PCL/Gel nanofiber, the 14% (wt/v) polycaprolactone (PCL) and 20% (wt/v) gelatin solutions were prepared separately. A mixture of formic acid and acetic acid (1:9) was used as the solvent. Then both solutions were mixed at the ratio of 50:50. The process of electrospinning was performed at the flow rate of 0.5 mL/h, 20 kV voltage, and a distance of 12 cm between the nozzle and collector for 6 hours.

In this experiment, PCL/Gel nanofibers containing 5%, 10%, and 15% MnO2 nanoparticles were fabricated. Different concentration of MnO2-NPs (5, 10, and 15%) was added to the PCL/Gel solution and stirred overnight. Then the electrospinning process was conducted.

To cross-link the nanofibers, they were attached to the inner wall of a desiccator containing 25% glutaraldehyde. The desiccator was put in a 45 °C oven for 24 hours. Nanofibers were crosslinked in the glutaraldehyde vapor.

Scanning electron microscopy

The scanning electron microscopy (SEM) images of the morphologies of gold-sputter-coated MnO2 nanoparticles and electrospun nanofibers were acquired after being coated. (SEM; FEI, Quantum 450, USA). The diameter of

nanofibers and MnO2 nanoparticles was measured using ImageJ software (National Institutes of Health, USA). For MnO2 nanoparticles and each of the nanofibers, one hundred diameter measurements were performed on different regions of the SEM images. The diameter distribution histograms were generated by Origin 2022 software. Also, the obtained data were fitted with Gaussian distribution.

Energy dispersive X-ray spectrum (EDX) analysis was used to assess the presence and distribution of MnO2 nanoparticles in nanofibers.

Fourier transform infrared spectroscopy

Fourier transform infrared spectroscopy (FT-IR) spectrum of PCL, Gelatin, and MnO2 NPs, and the chemical interaction of different functional groups were revealed by FT-IR spectrophotometer (IR prestige-21, Shimadzu Co., Japan) using potassium the bromide disk method. The scanning range was 400–4000 cm^{-1} with a spectral resolution of 4 cm^{-1}. 5–6 mg of samples were mixed and triturated with potassium bromide (100 mg) and placed in the sample holder.

Mechanical properties

The mechanical characteristics of different nanofibers were determined using the tensile strength method, following the ISO 5270:1999 standard test techniques. Tensile testing was performed at a strain rate of 1 mm per minute using a uniaxial tensile testing apparatus (Santam, Iran). For each nanofiber, the stress-strain curve was reported.

Contact angle

To determine the hydrophobic/hydrophilic nature of the nanofibers, the water contact angle was evaluated with a static contact angle goniometer (Jikan CAG-20, Jikan Surface Nano-Engineering Company, Iran). In each sample, the deionized water droplet (5 µL) was poured onto three different points. Contact angles between the droplet and the sample surface were measured via Jikan Assistant software. The average angle was reported.

Porosity

The liquid displacement process was used to assess the nanofiber's porosity. Briefly, the samples were soaked in hexane until they reached saturation. Once all trapped air had been eliminated, the samples were removed from hexane. Tests were performed in triplicate. Equation 1 was used to calculate the porosity.

$$Porosity\ (\%) = (W2 - W1 / W2 - W3) \times 100 \quad (1)$$

Where W1 is the weight of dry nanofiber in the air, W2 is the weight of hexane-impregnated nanofiber in the air, and the weight of nanofiber suspended in hexane is indicated by W3.[28]

Swelling test

The swelling tests were conducted in distilled water. Briefly, dry nanofiber samples (1 cm × 1 cm) were weighed and then submerged in distilled water. After the specified time, samples were removed from the water using spatulas, excess water was collected using tissue paper, and samples were weighed again. Monitoring of the nanofiber's swelling was performed until equilibrium in weight gain was achieved. The following formula was used to calculate the swelling ratio:

$$Swelling\ ratio = [(W - W_0)/W_0] \times 100$$

where W0 and W refer to the weights of dry and swollen samples, respectively.

Biodegradability test

An *In vitro* degradation test of the prepared nanofibers was conducted in PBS on days 7,14, 21, and 42. Briefly, each nanofiber was cut into 1 × 1 cm^2 pieces and the initial weight (W0) was measured and then submerged in 3 mL PBS. The samples were removed from the PBS at certain intervals and dried at 45 °C for 24 hours before being weighed. (W1). All the biodegradability tests were performed in triplicate. The percentage of weight loss was calculated using the following equation:

$$Weight\ loss\ (\%) = (W0 - W1/ W0) \times 100$$

The morphology of degraded nanofibers was also observed using SEM photography.

Blood compatibility

The hemocompatibility test was performed using human fresh anticoagulated blood diluted with normal saline (1:1). Nanofibers were punched and incubated with 150 µL of the diluted blood for 60 minutes at 37 °C before centrifugation at 1500 rpm for 10 minutes. The absorbance of the supernatant was measured at 545 nm by a microplate reader (BioTek, Synergy H1, USA). Blood diluted with normal saline (1:1) and blood diluted with deionized water (1:1), were accounted as the negative and positive controls, respectively. Equation 2 was used to calculate the hemolysis percent:

$$Hemolysis\ (\%) = (Dt - Dnc / Dpc - Dnc) \times 100 \quad (2)$$

Where Dt, Dnc, and Dpc are the sample, negative control, and positive control absorbances, respectively.

Isolation, expansion, and characterization of ADSC

Rat ADSCs were extracted from fresh subcutaneous adipose tissue of male Wistar rats. The adipose tissue was isolated under sterile circumstances, rinsed with phosphate-buffered saline (PBS; Kiazist Life Sciences, Iran) containing 5% penicillin/streptomycin (pen/strep),

and cut into small pieces. Then, enzymatic digestion was performed with 1 mg/mL collagenase type I solution in PBS followed by incubation and shaking at 37 °C for 2 hours. Centrifugation was carried out at 800 ×g for 5 minutes following collagenase neutralization using DMEM (Kiazist Life Sciences, Iran) containing 10% fetal bovine serum (FBS; Gibco). The cell pellet was cultured in DMEM supplemented with 10% FBS and 1% pen/strep (Kiazist Life Sciences, Iran) at 37 °C, 98% humidity, and 5% CO2.[29] ADSCs of passage four were used for all experiments.

Immunophenotyping of rat ADSCs

The surface markers of ADSCs were assessed using flow cytometry analysis. Fourth-passage cells were trypsinized and resuspended in PBS at a density of 1×10^5 cells per 1.5 mL. ADSCs were incubated with the FITC-conjugated antibodies for 2 hours at room temperature. Anti-CD73, anti-CD45, anti-CD34, anti-CD105 and CD90 antibodies were used (1:50; all from BIOSS). After two PBS washes, a flow cytometer was used to evaluate the cells (Attune NxT, Thermo Fisher Scientific, USA).[30]

Tri-lineage differentiation

The ADSCs capacity of tri-lineage differentiation including adipogenesis, osteogenesis, and chondrogenesis was evaluated. Rat ADSCs at the fourth passage with 80-90% confluency were used for cell differentiation analysis. ADSCs differentiation was induced using adipogenic, osteogenic, and chondrogenic differentiation kits (Cyagen Bioscience Inc., Guangzhou, China) based on the manufacturer's instructions. Alcian Blue (chondrogenic), Alizarin Red (osteogenic), and Oil Red O (adipogenic stains were used to confirm the tri-lineage distinction.

Cell viability assay

The viability and proliferation of ADSCs on the nanofibers were determined using the 3-(4,5-dimethylthiazol-2-yl)-2,5-diphenyl tetrazolium bromide (MTT) test. Nanofibers were cut into 1×1 cm^2 squares, sterilized via ultraviolet (UV) irradiation and immersion in 70% ethanol, washed thrice with PBS, and incubated with DMEM medium for 24 hours. Then, 2 $\times 10^4$ ADSCs were seeded on the nanofibers. MTT solution was introduced to the wells after 24, 48, and 72 hours and incubated for 4 hours before the absorbance was measured at 570 nm.

ADSCs adhesion and morphology analysis

To assess the cell adhesion and morphology on the scaffold, the SEM image of ADSCs seeded on the Mn-5% nanofiber (the final selected scaffold) was obtained. To this end, 2 $\times 10^4$ ADSCs were seeded on the 1×1 cm^2 nanofiber according to the steps mentioned in the MTT assay.

The cells seeded on the nanofiber were washed three times with PBS after the 48-hour incubation period, then fixed for 2 hours at room temperature with a 2.5% glutaraldehyde solution, and then rinsed again with PBS. The sample was subsequently dehydrated for 10 minutes in gradient concentrations of ethanol (50%, 70%, 80%, 95%, and 100%), freeze-dried, and the SEM image was recorded.

Burn model

First, 15 male Wistar rats (200 g) were anesthetized with ketamine (10%, 100 mg/kg BW) and xylazine (2%, 10 mg/kg BW) intraperitoneally. The second-degree burn model was developed using the approach described in the publication of Cai et al publication.[31] The device which was used to create the burn model has a circular metal disk of 1.5 cm diameter, that is heated to a temperature of 100 °C using an electrical heating element. To create a burn model, this device was placed vertically on the rat skin (on its weight) for 10 seconds. Around the burn wound, the piroxicam was injected subcutaneously (5 mg/kg). Rats were anesthetized one day after the burn model was created, and nanofibers (seeded with 3×10^6 ADSCs (N+S/Mn+S groups) or without cells (N/Mn group)) were sutured to the wound sites. Wounds were covered with a piece of sterile gauze impregnated with PBS (containing 1% pen/strep and 1% amphotericin B) and then a transparent adhesive bandage (good air permeability) was used. The group model abbreviation is according to below:

In vitro assays

Mn-0%: PCL/Gelatin nanofiber

Mn-5%: Nanofiber (PCL/Gelatin/ 5% MnO2 nanoparticles (NPs))

Mn-10%: Nanofiber (PCL/Gelatin/ 10% MnO2 NPs)

Mn-15%: Nanofiber (PCL/Gelatin / 15% MnO2 NPs)

In vivo assays

Control: No treatment

N: Nanofiber (PCL/Gelatin)

Mn: Nanofiber (PCL/Gelatin/ 5% MnO2 NPs)

N+S: Nanofiber (PCL/Gelatin) + Stem cell (ADSCs)

Mn+S: Nanofiber (PCL/Gelatin/5% MnO2 NPs) + Stem cell (ADSCs)

Wound closure rate

The wound closure rate was determined by imaging the wound on days 0 and 21 post-burn induction. The wound area was measured using the ImageJ software. The following formula[32] was used to calculate the percentage of wound closure:

Percentage of wound closure = [(wound area on day 0 - wound area on day 21) / wound area on day 0] × 100

On day 21, the rats were sacrificed under ether anesthesia to collect skin biopsies from the burn site for further analysis. Excised skin was divided into four pieces. One part was fixed in 10 % formaldehyde for histological studies; The remaining three parts were kept in microtubes

at -80°C until use for ELISA (IL-1, IL-6), hydroxyproline, and glycosaminoglycan (GAG) analysis.

Enzyme-linked immunosorbent assay

The level of IL-1β and IL-6 in the burn wound area was determined using Enzyme-linked immunosorbent assay (ELISA) kits (Karmania Pars Gene Company Kerman, Iran) according to the manufacturer's instructions.

The total protein content was estimated using the BCA protein assay kit (Kiazist Life Sciences, Iran) by the instructions of the manufacturer to normalize the amounts of IL-1 and IL-6.

Hydroxyproline and glycosaminoglycans content

The hydroxyproline content of the skin samples was measured using a hydroxyproline assay kit (Kiazist Life Sciences, Iran) based on the instructions of the manufacturer. Moreover, the dry weight of samples was used to normalize the data.

The amount of GAGs present in the healed skin was determined using the GAG assay kit (Kiazist Life Sciences, Iran) based on the manufacturer's instructions. The concentration of GAGs was calculated using the chondroitin sulfate standard curve. Also, the DNA concentration of samples was used to normalize the data.

Haematoxylin and eosin and Masson's trichrome staining

A series of graded ethanol solutions were used to dehydrate the fixed 10% formalin skin specimens. Samples were then washed in xylene and embedded in paraffin. Sections of 5 m thickness were cut and stained with hematoxylin and eosin (H&E) and Masson's trichrome (MT). Finally, the stained slides were evaluated by an optical microscope (Olympus).

Immunohistochemistry staining

Immunohistochemistry (IHC) staining was used to identify the positive expression of α-SMA in the skin tissue. This staining was conducted on 5 μm sections of paraffin-embedded skin specimens using an α-SMA IHC kit (Medaysis Company, USA; Zytomed Systems, Germany) based on the instructions of the manufacturer.

Statistical analysis

GraphPad Prism 9 (version 9.0.0 (121), USA) was used to analyze the data using one-way or two-way analysis of variance (ANOVA) and the post hoc Tukey's test. The results are reported as mean standard deviation (SD), and a $P<0.05$ level of significance was considered statistically significant.

Results

Characterization of MnO2-NPs

The surface shape and size of MnO_2-NPs were determined using SEM images (Fig. 1A). According to the histogram and SEM image, the synthesized manganese dioxide nanoparticles have favorable size, Poly Dispersity Index (PDI), and morphology (spherical shape) with a mean particle size of 46.91 nm (Fig. 1B).

Morphology of nanofibers

According to SEM images (Fig. 1C), the nanofibers are almost uniform fibers without beads and deformities and MnO_2-NPs are easily detectable. The presence of these nanoparticles in the nanofiber may be more clearly detected by increasing the nanoparticle concentration. Based on the results of this analysis, adding nanoparticles to nanofibers and increasing the concentration of nanoparticles did not have an adverse impact on the morphology of nanofibers.

SEM image analysis with ImageJ and Origin 2022 software indicates that the mean diameter of nanofibers with 5%, 10%, and 15% nanoparticles are 548.838, 834.622, and 912.158, respectively. Fiber diameter distribution histograms are presented in Fig. 1D. The average diameter of nanofiber without MnO2 NPs (Mn-0%, 1440.849) is higher than the mean diameter of nanofibers containing MnO2-NPs.

X-ray energy dispersive spectroscopy

The presence of nanoparticles in the structure of the nanofibers was confirmed by EDS point and map analysis. Since the oxygenated species are manganese dioxide, by increasing the percentage of nanoparticles, the concentration of manganese and oxygen atoms has increased (Supplementary file 1, Fig. S1).

FTIR spectroscopy analysis

The PCL/Gel/MnO_2 NPs nanofiber was synthesized through the reaction of the amine group of Gel and OH group of MnO_2. The spectrum of PCL (Fig. S2) revealed sharp bands at 1732 cm^{-1} which was characteristic of the C=O stretching vibration of the ester, and the peaks at 1180 and 1045 cm^{-1} were related to the C-O stretching vibration of the ester. Also, the sharp peak at 3099 cm^{-1} described C-H cycloalkane of PCL, and the peaks at 2927 and 2862 cm^{-1} corresponded to C-H symmetric and asymmetric stretching vibrations.

The gelatin spectrum (Fig. S2) showed peaks at 3402, 3043, 2927, 2854, 1685, 1604, and 1118 cm^{-1}. The broad peak at 3402 cm^{-1} was a feature of OH and NH stretching vibration. The peaks at 2927 and 2854 cm^{-1} corresponded to C-H aliphatic stretching vibration. The peaks at 1734 and 1654 cm^{-1} were a feature of the C=O stretching vibration group of the ester and amid from Gel, respectively. The peaks at 1639 (N-H bending vibration of primary amine) and 1564 cm^{-1} (N-H bending vibration of second amine) disappeared. The peak at 1544 cm^{-1} corresponded to -N=C- stretching vibration of Gel. Also, the peaks at 1170 and 1047 cm^{-1} were related to C-O stretching vibration.

The spectrum of MnO_2 NPs (Fig. S2) showed the peaks at 3423, 2924, 2854, 1739, 1633, 1389, 1111 and 636

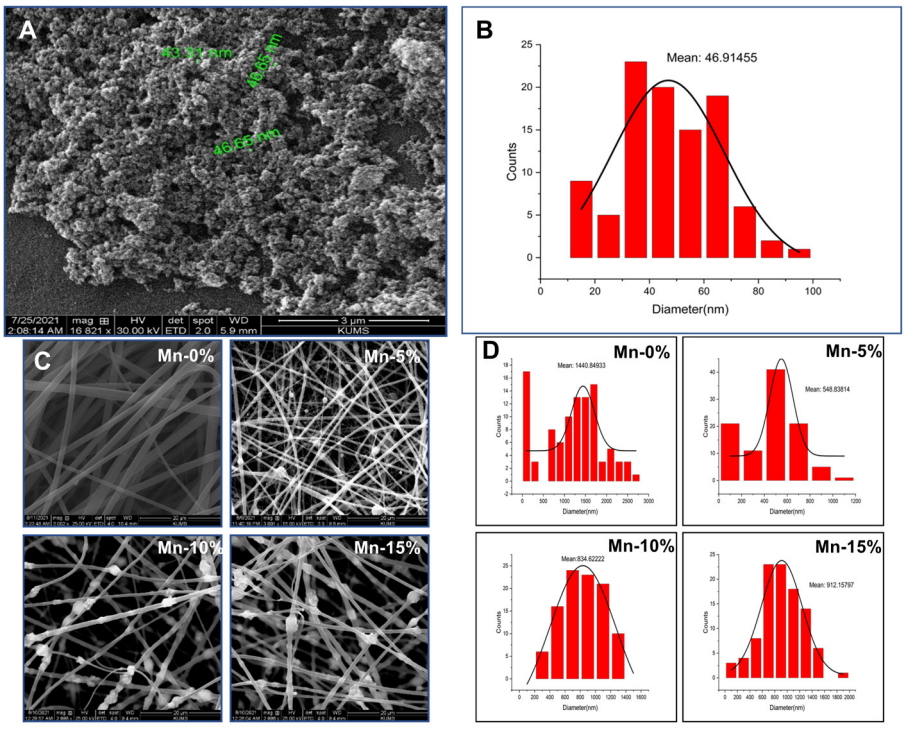

Fig 1. (A) SEM image of MnO2-NPs. (B) Histogram of diameter distribution of MnO2-NPs. (C) SEM image of nanofibers. (D) Histogram of diameter distribution of nanofibers.

cm^{-1}. The broad peak at 3423 cm^{-1} was a feature of OH stretching vibration. The sharp peaks at 1389 and 636 cm^{-1} were a feature of Mn-O stretching vibration and bending vibration of MnO_2 NPs.[33]

Fig. S2 indicates the IR spectrum of PCL/Gel/MnO2 NPs nanofiber. This spectrum revealed sharp bands at 3287, 2943, 2866, 1726, 1643, 1588, 1458, 1344, 1396, 1294, 1240, 1170, 1047 and 655 cm^{-1}. The sharp peaks at 2943 and 2866 cm^{-1} were a feature of C-H symmetric and asymmetric stretching vibrations of PCL, Gel, and MnO2 NPs. The sharp peaks at 1726 and 1643 cm^{-1} described the C=O ester and amide stretching vibration of PCL and Gel. The peak at 1588 was a feature of the NH second amine bending vibration of the Gel unit. The peaks at 1396 and 655 cm^{-1} were a feature of Mn-O stretching vibration and bending vibration of MnO_2 NPs. Also, the peaks at 1174 and 1047 cm^{-1} were a feature of the C-O stretching vibration of the ester from the PCL and Gel unit.

The presence of peaks at 1726 and 1643 cm^{-1} correlated to C=O from the PCL and Gel group, and the peak at 1588 cm^{-1} was a feature of N-H second amine bending vibration of the Gel which can confirm the synthesis of PCL/Gel/MnO2 NPs nanofiber. Also, the presence of the peaks at 1344 and 655 cm^{-1} was a feature of Mn-O stretching vibration and bending vibration of MnO_2 NPs which can confirm the synthesis of PCL/Gel/MnO2 NPs nanofiber. In addition, the omitted sharp peak at 3423 cm^{-1} corresponded to the OH of MnO_2 NPs and NH primary amine of Gel, which confirms the synthesis of PCL/Gel/MnO_2 NPs nanofiber. Also, the FT-IR spectrum of PCL/Ge/MnO_2 NPs nanofiber showed prominent shifting of its peaks in comparison to those of PCL, Gel, and MnO_2 NPs. The changes in the peak positions were observed in 1732 to 1726, and 636 to 655 cm^{-1}. These results confirmed the presence of PCL, Gel, and MnO_2 NPs in the spectrum of PCL/Gel/MnO_2 NPs nanofiber. Also, the peaks in the spectrum of PCL/Gel/MnO_2 NPs nanofiber had lower intensity than the peaks of PCL, Gel, and MnO_2 NPs.

Tensile strength

The mechanical test findings show that the nanofiber without nanoparticles has a high elongation percent, low UTS, and high elasticity. As a result of adding the MnO_2-NPs, the mechanical characteristics of the nanofiber have changed. In nanofibers containing nanoparticles, the elasticity and the percentage of elongation have decreased and the UTS value has remarkably increased (Fig. S3). During our animal experiments, the Mn-5% nanofiber was determined to be an appropriate choice for use as a wound dressing. This nanofiber has good elasticity and tensile strength, and it maintains its original structure throughout the wound-healing process.

Water contact angle

The water contact angle of nanofibers was determined to determine the hydrophilic/hydrophobic characteristics of scaffolds.

Our results demonstrate that the contact angle of the nanofiber without nanoparticles is less than 90 degrees, indicating the hydrophilic nature. The water contact

angle of nanofibers increases (above 90 degrees) with the addition of MnO2 nanoparticles compared to the Mn-0% nanofiber, showing that these nanoparticles decrease the hydrophilic property of nanofiber. However, the hydrophilic characteristic of Mn-5% nanofiber (the final selected scaffold for animal study) was slightly reduced (Fig. 2A, C).

Porosity

In nanofibers containing nanoparticles, the percentage of porosity has increased significantly compared to the nanofibers without nanoparticles. Among the nanofibers containing 5, 10, and 15% nanoparticles, there is no significant difference in terms of porosity (Fig. 2B) (P>0.05).

Water absorption test (swelling test)

Based on the results of the swelling test, in nanofibers containing MnO_2-NPs, the percentage of swelling has significantly increased compared to the nanofibers without nanoparticles. The addition of MnO2 nanoparticles to the nanofiber structure increased porosity and, as a result, increased water absorption rate (Fig. 2D).

Biodegradability analysis and weight loss

The SEM images of the degraded samples and the graph of the weight loss on different days are shown in Fig. 3. According to the SEM images, the diameter of the nanofibers has increased over time, and the type of nanofiber structure has shifted from fibrous to ribbon form. Indeed, nanofibers have hydrolyzed and fused. As a result, the rate of biodegradability has increased in all types of nanofibers over time. ANOVA statistical analysis showed that the incorporation of nanoparticles into the nanofiber structure significantly increased the weight loss or degradation rate compared to the Mn-0% nanofibers. Moreover, by increasing the percentage of nanoparticles, the degradation rate has also increased (Fig. 3A).

Blood compatibility

The results of the hemocompatibility tests revealed that none of the nanofibers induced significant hemolysis (Fig. 4A).

Immunophenotyping of ADSCs

Flow cytometry analysis was used to evaluate the expression of MSCs-specific cell surface markers (CD105, CD73, CD90) and hematopoietic markers (CD45, CD34). The findings revealed that a high percentage of cells expressed CD105, CD90, and CD73 markers (97.2, 94.2, and 94.4, respectively), whereas a minor number of cells exhibited CD45 and CD34 markers (3.4% and 1.8%, respectively) (Fig. 4B).

Tri-lineage differentiation

Oil red O, alcian blue, and alizarin red staining revealed

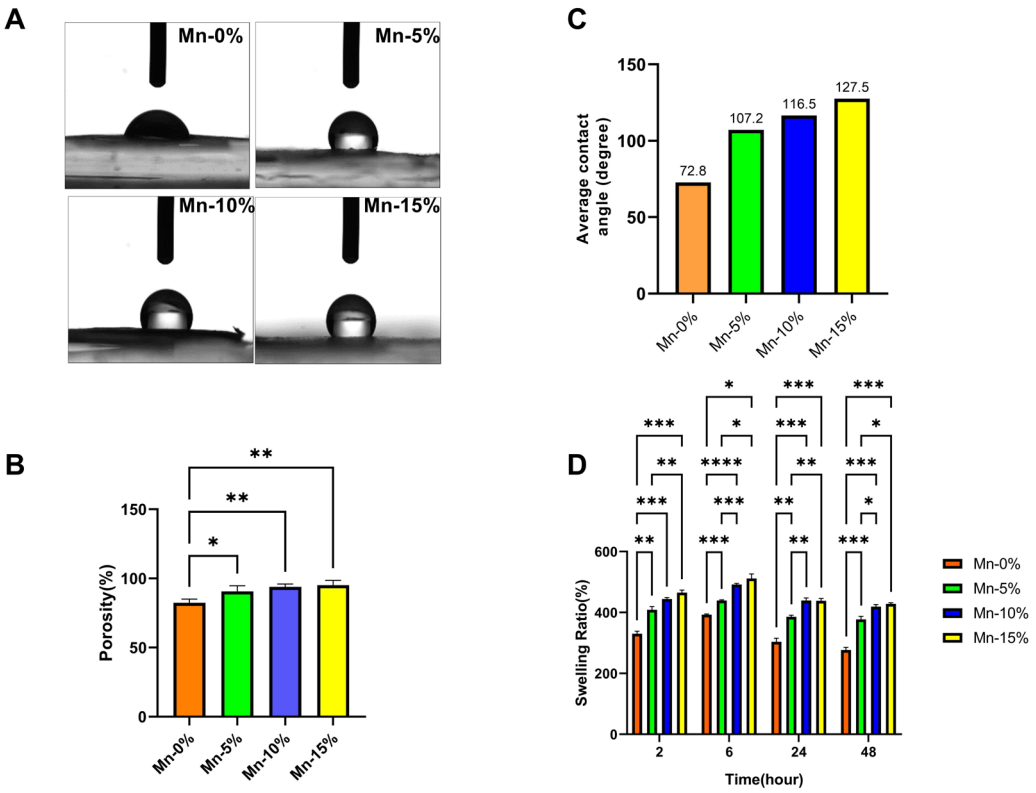

Fig 2. (A) The water contact angle of nanofibers. (B) The average contact angle of nanofibers. (C) Porosity (%) of nanofibers (D) Swelling ratio (%) of nanofibers.

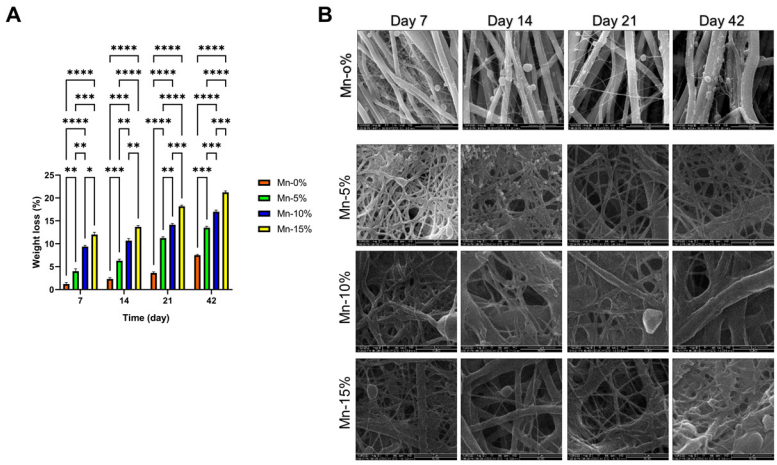

Fig 3. (A) weight loss (%) of nanofibers. (B) SEM images of degraded samples.

that the isolated ADSCs had the capacity of adipogenic, chondrogenic, and osteogenic differentiation. Flow cytometry analysis and differentiation results indicated that ADSCs were successfully isolated from the rat adipose tissue and could differentiate into three lineages fat, cartilage, and bone (Fig. 4C).

Cell viability assay

The MTT test findings demonstrated that the addition of 5% nanoparticles to the nanofiber structure (Mn-5%) had no significant influence on the viability and metabolic activity of ADSCs compared to nanofiber without nanoparticles. The absorption rates of these two groups were nearly identical at 24, 48, and 72 hours. In comparison to the Mn-0% and Mn-5% groups, increasing the percentage of nanoparticles to 10% and 15% resulted in a significant drop in cell viability at 24, 48, and 72 hours (P<0.05). In the Mn-15% group, the cell viability was significantly reduced at 48 and 72 hours in comparison to the Mn-10% group (Fig. 4D).

Cell adhesion assay

According to the results, ADSCs have favorable adhesion and growth on the Mn-5% scaffold, and the mitotic process can be easily observed. Furthermore, ADSCs are attached to the scaffold in a three-dimensional manner, demonstrating that the constructed scaffold creates an appropriate condition for cell growth and proliferation that is similar to the environment seen in the body (in vivo).

Based on the findings of different tests conducted on nanofibers, the most suitable scaffold for animal investigations was found to be the nanofiber containing 5% MnO2 NPs (Mn-5%). ADSCs seeded on the Mn-5% scaffold were utilized for animal study (in vivo) (Fig. 4E).

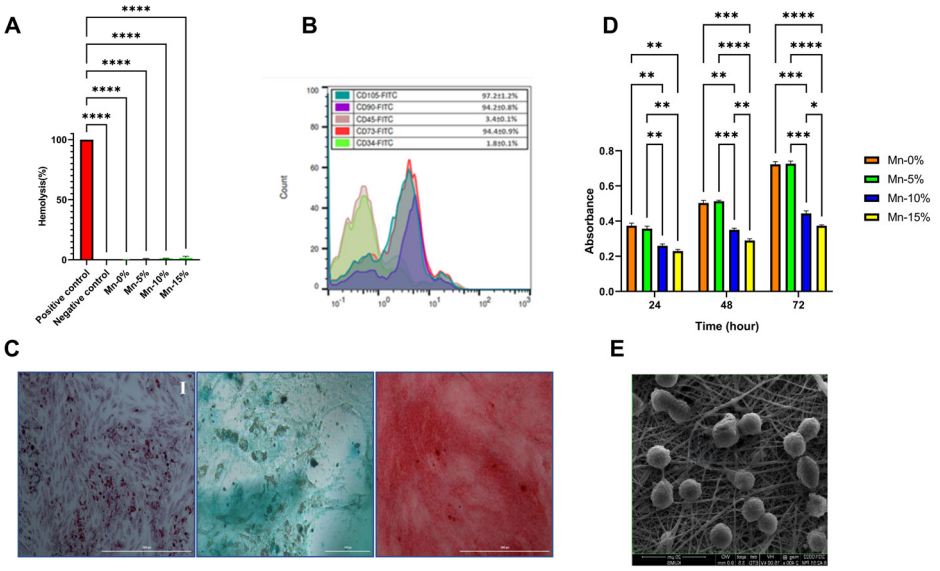

Fig 4. (A) Blood compatibility tests. (B) Flow cytometry analysis of ADSCs. (C) Tri-lineage differentiation of ADSCs: (I) Oil Red O (adipogenic), (II) Alcian Blue (chondrogenic), and (III) Alizarin Red (osteogenic) staining. (D) Cell viability assay. (E) Cell adhesion assay (Mn-5% nanofiber).

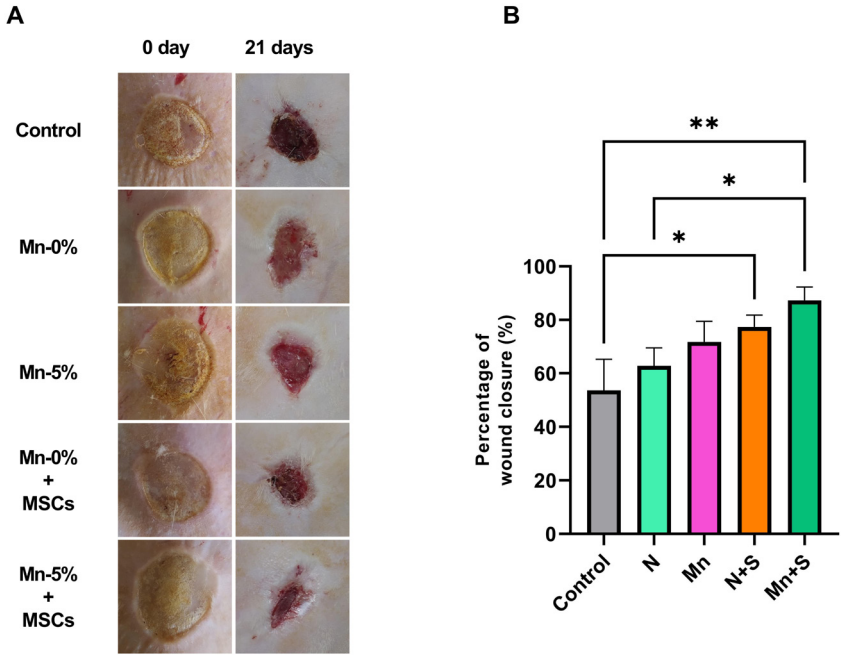

Fig 5. (A) Representative photographs of wounds on days 0 and 21. (B) The percentage of wound closure.

In vivo evaluations

Wound closure

The results of Fig. 5 show that the control group had the lowest percentage of wound closure. The wound closure percentage was increased in the Mn and N groups in comparison with the control group (without treatment) and the Mn group compared to the N group, although the difference was not statistically significant ($P > 0.05$). Also, the percentage of wound closure was significantly raised in the Mn+S and N+S groups than in the control group. In these two groups, wound healing was faster than in the other groups. In the Mn+S group, the wound closure increased in comparison to the N+S group, but this increase was not significant. In addition, the wound closure percentage was higher in the Mn+S group compared to the N group (P <0.05) (Fig. 5).

Inflammatory factors (IL-1 and IL-6)

The IL-1 and IL-6 level in the N and Mn groups was lower compared to the control group, although was not significant. The level of these two factors in the Mn+S and N+S groups decreased significantly compared to the control group. Although IL-1 and IL-6 levels were lower in the Mn+S group than in the N+S group, the difference was not statistically significant. In the Mn+S group compared to the N group, as well as in the Mn+S group compared to the Mn group, the levels of IL-1 and IL-6 were significantly reduced. (Fig. 6A, B).

Hydroxyproline content

According to the findings, there is an increase in the quantity of hydroxyproline in the N and Mn groups in comparison to the control group, and in the Mn group compared to the N group, although the difference between

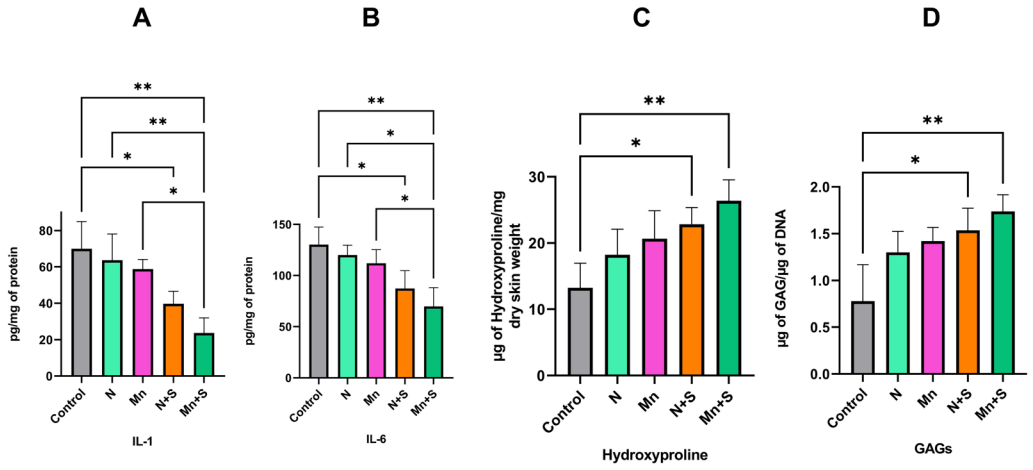

Fig 6. (A) The levels of IL-1(A) and IL-6 (B). Hydroxyproline (C) and Glycosaminoglycans (D) content.

the groups is not statistically significant. Compared to the control group, the quantity of hydroxyproline in the N+S and Mn+S groups has increased significantly. Furthermore, as compared to the N+S group, the quantity of hydroxyproline in the Mn+S group has increased, although this increase is not significant (Fig. 6C)

Glycosaminoglycans content

As shown in Fig. 6D, the quantity of glycosaminoglycan was increased in the N and Mn groups in comparison to the control group, and in the Mn group compared to the N group, although this increase was not statistically significant. Compared to the control group, the amount of glycosaminoglycan in the N+S and Mn+S groups has a significant increase. The Mn+S group has more glycosaminoglycan content than the N+S group, although the difference is not statistically significant (Fig. 6D).

H&E and Masson's trichrome staining

Different parts of healthy skin, the epidermis (E), and dermis (D) with appendages and the connective tissue fibers along with cells are detectable. The tissue structure was irregular and unclear in the control group, the necrotic tissue (N) was developed in the surface area of the wound, inflammatory phase cells were present under the necrotic tissue, and the collagen fibers had less density and were irregular in the extracellular matrix.

Tissue disorganization was decreased in the N treatment group in comparison to the control group. Also, less inflammatory cells and necrotic tissue were observed. In the Mn group, tissue alterations were improved compared to the N group. As a consequence, the necrotic tissue and the inflammatory cell accumulation were decreased, and the collagen fibers were detected. The results indicate that in the S+N group, the skin damage was reduced in comparison to the control, N, and Mn groups. Also, the epidermis was formed in a band shape in a wide area, and the connective tissue cells and filaments appeared normal. In the Mn+S group, the skin tissue structure was improved compared with the other treatment groups and had better treatment status. Overall, no skin appendages were detected at the site of tissue injury, in any of the groups (Fig. 7).

Immunohistochemical staining for α-SMA

According to the results of immunohistochemical staining, the level of α-SMA in the control group is higher

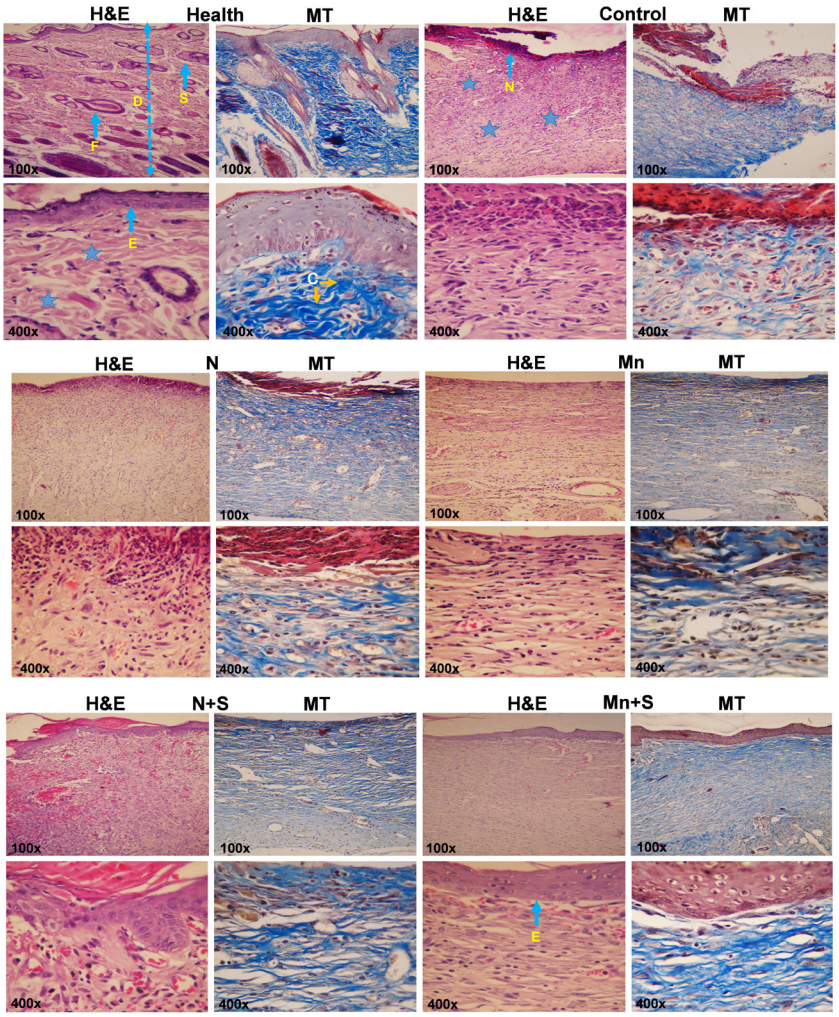

Fig 7. Representative images of skin sections stained with H&E and Masson's trichrome (MT) (F: hair follicle, D and asterisk: Dermis, S: Sebaceous glands, E: Epidermis, C: collagen fibers, N: Necrosis).

than in all other groups. Considering that the wound closure percentage in the control group is less than in other groups, there is a higher amount of α-SMA to help the wound closure.

The amount of α-SMA in the N group is lower than in the control group, and also in the Mn group is less than in the N group. The presence of MnO2 nanoparticles in the nanofiber structure has reduced the amount of α-SMA. The lowest amount of α-SMA is observed in the Mn+S and N+S groups. In these two groups, the wound closure percentage was higher than in the other groups, therefore, the level of α-SMA has decreased and, subsequently, the possibility of fibrosis formation has been prevented.

In the Mn+S and N+S groups, ADSCs inhibited fibrosis formation by reducing the α-SMA levels. The amount of α-SMA in the Mn+S group is lower than in the N+S group and, is closer to healthy skin. The treatment in the Mn+S group was better than all other groups. Indeed, the presence of MnO2 nanoparticles in the nanofiber and stem cells in this group has made the treatment more appropriate and faster (Fig. 8).

Discussion

According to the SEM images, due to the addition of 5% MnO2 nanoparticles, the diameter of nanofibers has significantly decreased compared to the Mn-0% nanofibers. The inclusion of nanoparticles in the solution caused a buildup of high charge density on the ejected jet surface and a significant increase in total electric charges during electrospinning. As a result, the diameter of the nanofibers was decreased.[34,35] In addition, by increasing the percentage of MnO2-NPs to 10% and 15%, the diameter of nanofibers has increased compared to Mn-5% nanofiber, owing to an increase in the solution viscosity. These findings are similar to the findings of the Mpukuta et al research, which revealed enhanced nanofiber diameters by increasing the percentage of nanoparticles.[36]

In the SEM images, the MnO2 NPs can be detected in the nanofiber structure. EDX analysis additionally identified the presence of MnO2 NPs in the PCL/Gel nanofiber. The results of mechanical tests showed that the nanofiber without nanoparticles has a high elongation percent, low UTS, and high elasticity. While, in the nanofibers containing nanoparticles, the elasticity

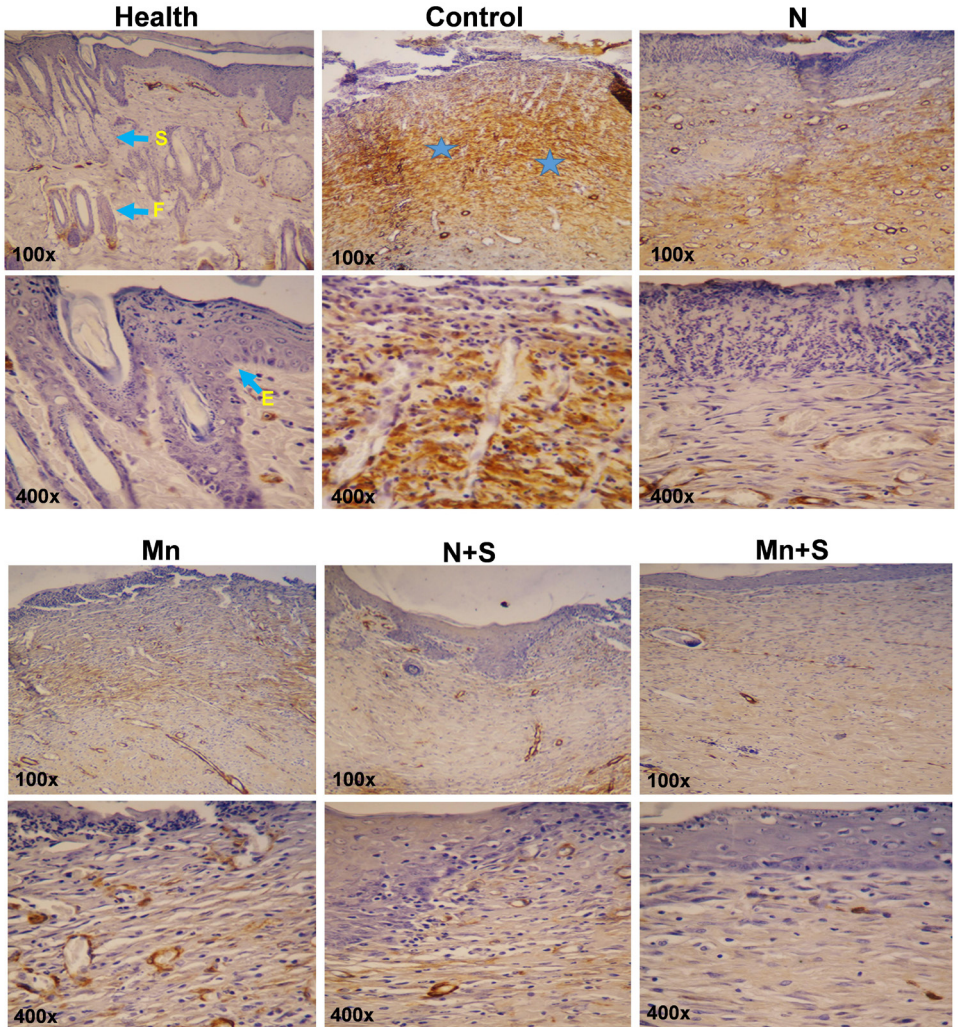

Fig 8. Immunohistochemistry staining of a-SMA (F: hair follicle, asterisk: Dermis, S: Sebaceous glands, E: Epidermis).

and the percentage of elongation have reduced and the UTS value has remarkably increased. Our findings are consistent with previous studies. Hivechi et al synthesized polycaprolactone–gelatin hybrid nanofibers and incorporated cellulose nanocrystals (CNC) into the nanofibers to improve their characteristics. The results of the mechanical test indicated that CNC incorporation caused a significant increase in tensile strength and modulus ($P<0.05$).[37] According to Augustine et al.[38] results, the addition of a high concentration of nanoparticles (0.5%) to scaffolds reduced the elasticity due to high surface energy and easy aggregation of nanoparticles.

Our results demonstrate that the contact angle of the nanofiber without nanoparticles is less than 90 degrees, indicating the hydrophilic nature. The addition of MnO2 nanoparticles raises the water contact angle of nanofibers (above 90 degrees) compared to the Mn-0% nanofiber, indicating that these nanoparticles decrease the hydrophilic characteristic of nanofiber. Indeed, the addition of MnO2 nanoparticles to the structure of nanofiber increases the surface roughness of the nanofiber, and as a result, raises the water contact angle (decreases the hydrophilicity nature). However, the hydrophilic characteristic of Mn-5% nanofiber (the final selected scaffold for animal study) was slightly reduced. In accordance with the present results, previous studies have indicated that the addition of nanoparticles to polymeric solutions can change the surface characteristics of the scaffolds. Jiang et al indicated that the surface roughness of PVDF nanofiber increases by adding the Fe3O4 nanoparticles, therefore the hydrophobicity characteristic of the membrane increases.[39]

Dressings with higher porosity are useful in absorbing excess exudates and increasing the gas and liquid exchange at the wound sites.[40] The results of the current study showed that the diameter of the nanofibers dropped when MnO2 nanoparticles were added, and as a result, the percentage of porosity was increased. These results reflect those of Yanilmaz et al who explained that the higher porosity can be attributed to the reduced fiber diameter and increased roughness caused by increasing SiO2-NP concentration.[41]

The dressing materials should have a great capacity for water absorption to absorb wound secretions and keep the wound environment moist.[42] We indicated that the addition of MnO2 nanoparticles into the nanofiber structure increased the porosity and, as a result, the water absorption rate was increased. This finding was also reported by Khorasani et al, who indicated that the vacancies and pores in the hydrogel network were increased, due to the increase of ZnO concentration. Thus the water absorption and swelling rate of hydrogel systems were increased.[43]

Biodegradation analysis demonstrated that the addition of MnO2 nanoparticles into the nanofiber structure caused a significant increase in the weight loss or degradation rate compared to Mn-0% nanofiber. The presence of nanoparticles in nanofibers reduces the interactions between polymer chains and therefore increases the degradation rate. Moreover, by adding nanoparticles, the porosity of the nanofibers has also increased, and more water has penetrated the fiber. As a result, the degradation rate has increased. This finding was also reported by Dosstmohammadi et al[44] who reported that PCL/GEL/ Selenium NPs had increased weight loss in comparison to PCL/GEL nanofibers. The reduced crystallinity of the scaffolds may be the cause of the high degradation rate of scaffolds containing Se nanoparticles.

Zhang et al[45] indicated that the PCL/Gel complex fibrous membrane with high fiber density could be a hopeful scaffold for the adhesion and growth of bone marrow stromal cells. Thus, the porous nature of the PCL/Gel fiber membrane with high fiber density may be suitable for cell adhesion and proliferation, and provides enough exchange of nutrients and gas for wound healing.

It is worth noting that no significant difference was seen in the viability of ADSCs seeded on nanofibers containing PCL/Gel and PCL/Gel/ 5% MnO2 NPs at 24, 48, and 72 h. This result is consistent with the findings of Doostmohammadi et al[44] who reported that no significant difference in cell proliferation was seen between cells seeded on PCL/GEL and PCL/GEL/Selenium NPs after 24, 48, and 72 hours. In our study, increasing the concentration of MnO2 nanoparticles to 10% and 15% caused a significant decrease in cell viability at 24, 48, and 72 hours in comparison to the Mn-0% and Mn-5% groups. Alipour et al[45] discovered a slight decrease in cell viability of HSFPI18 fibroblast cells seeded on PVA/PVP/Pectin/ Mafenide acetate scaffolds comprising 0.7% AgNPs. In another study, Aktürk et al[46] discovered a significant decrease (down to 67%) in the viability of 3T3 cells seeded on Au-containing collagen/PEO nanofibres.

As wound dressings interact with blood, particularly in severe burn damage, hemocompatibility is an essential feature.[47] All of our synthesized nanofibers had no hemolytic effects. These findings are consistent with earlier research which demonstrated the high hemocompatibility of PCL and PCL/Gel nanofibers.[48]

IL-6 and IL-1, which are proinflammatory mediators, are essential in stimulating the formation of scars. In the present study, the use of nanofibers containing PCL/ gelatin, 5% MnO2 NPs, and ADSCs as wound dressing led to a significant reduction in the inflammatory responses. The IL-1 and IL-6 levels in the N+S and Mn+S groups were significantly decreased compared to the control group. In addition, the amount of these interleukins in the Mn+S group has significantly decreased compared to the N group. Considering that these factors in the N+S group have not decreased significantly compared to the N group, it can be concluded that the treatment with the combination of MnO2-NPs and ADSCs is effective in the significant reduction of IL-1 and IL-6 levels. According

to these findings, which are in line with earlier studies, ASCs have anti-inflammatory impacts by reducing pro-inflammatory cell recruitment as well as decreasing inflammatory cell activation and growth.[49] It has been demonstrated that entering an inflammatory environment and being exposed to inflammatory cytokines such as interferon-gamma, IL-1, and tumor necrosis factor-alpha activates the immunomodulatory phenotype of mesenchymal stem cells.[50]

Reducing the pro-inflammatory cytokines minimizes/prevents hyper granulation tissue and fibrosis formation. Our findings are consistent with the findings of Liu et al,[51] who discovered that mesenchymal stem cell therapy reduced scar tissue formation through regulating the inflammatory cytokines. The results of the study by Manning et al[52] showed that there is minimal evidence to support the idea that ASCs can directly inhibit IL-1 production. They hypothesized that ASCs may regulate macrophage activity and encourage their transition to the M2 phenotype, which is a potential explanation for the decrease in pro-inflammatory cytokines and growth factors, including IL1 and TGF-1.

Mahdavi et al reported that MnNPs@ZC (manganese nanoparticles synthesized using *Ziziphora clinopodioides* Lam) ointment significantly reduced the wound area, the total number of cells, lymphocytes, and neutrophils, and caused a significant increase in wound closure, hexuronic acid, hexosamine, hydroxyl proline, fibrocytes, and fibrocytes/fibroblasts in comparison to other treatments. Based on the results of this experiment, the synthesized MnNPs@ZC showed dose-dependent antifungal, antibacterial (gram-positive and negative bacteria), antioxidant, non-cytotoxicity, and skin wound healing effects.[26]

In the present research, the percentage of wound closure, glycosaminoglycans, and hydroxyproline content in the Mn+S and N+S groups has significantly increased in comparison to the control group. The ADSCs-treated groups indicated a significant increase in the hydroxyproline expression, which proves the significant increase in collagen synthesis. These findings were previously presented by other studies, which reported that combining ASCs with Aloe vera and Honey can significantly promote the healing of burn wounds through stimulating mesenchymal cell proliferation, collagen formation, re-epithelialization, and angiogenesis.[53, 54]

The histology report of the current study indicates that the wound healing status and the tissue structure of the groups treated with PCL/Gel nanofibers (N group) were better than the control group, which was possibly owing to wound moisturization, wound protection from outside contamination, and the healing properties of gelatin.[55] In the Mn group, results demonstrated the reduction of necrotic tissue and inflammatory cells, as well as a rise in the collagen fibers in comparison to the N and control groups, proving the healing effects of MnO2 NPs. In the S+N and Mn+S groups, the skin damage was further reduced, the epidermis was formed in a band shape in a wide area, and the connective tissue cells and filaments appeared normal. Overall, the best type of treatment was observed in the Mn+S group. In this group, the skin tissue had the highest recovery rate and the best structure in comparison to other treatment groups. In line with these reports, Doostmohammadi et al demonstrated that the number of inflammatory cells was significantly reduced in the wounds treated with PCL/GEL/Selenium nanoparticles compared to the wounds treated with PCL/GEL and normal saline. Also, in the group receiving treatment with PCL/GEL/Se NPs/Vitamin E scaffold, full re-epithelialization, moderate inflammation, a mild degree of edema, low fibroblast density, and the maximum amount of collagen deposition were found.[44] Also, in another study, it was reported that the Aloe vera/ASCs treatment improved the re-epithelialization compared to other treatments on day 7 post-wounding. In addition, the histopathological investigations revealed more organized and altered bundles of connective tissue in the dermis of the Aloe vera/ASC-treated group in comparison to the rest of the groups after 28 days post-wounding.[54]

Fibroblasts enter the wound from the edges and also migrate toward the center in response to growth factors and cytokines. Some of these fibroblasts differentiate into myofibroblasts, which contain α-SMA and have enhanced contractile activity. Myofibroblasts help in wound closure by pulling their margins toward the center.[56] In our experiment, there is a reverse relationship between the wound closure percentage and the level of α-SMA. In the control group, the percentage of wound closure was less than in other groups, and therefore, there was a higher amount of α-SMA to help the wound closure. The amount of α-SMA in the Mn group was decreased compared to the control group and N group, indicating the role of MnO2-NPs in increasing the percentage of wound closure, decreasing the α-SMA expression, and reducing the possibility of scar formation. The highest rate of wound closure and the lowest amount of α-SMA was observed in the Mn+S and N+S groups, which demonstrate the greater role of stem cells in reducing α-SMA levels and thus preventing fibrosis. The amount of α-SMA in the Mn+S group is lower than in the N+S group and, is closer to healthy skin. The treatment in the Mn+S group was better than all other groups. Indeed, the presence of MnO2 nanoparticles in the nanofiber and stem cells in this group has made the treatment more appropriate and faster. The inverse relationship between the amount of α-SMA and wound healing is demonstrated by prior studies which found that a reduction in α-SMA after HMSC administration is related to optimal wound healing.[57]

Conclusion

In this study, MnO2-NPs were synthesized and the

Research Highlights

What is the current knowledge?

√ Stem cells and biomaterials are crucial in regenerative medicine. They are widely used for wound healing, with various nanoparticles and nanofibers.

What is new here?

√ For the first time, the combination of ADSCs and PCL/Gel/MnO2-NP nanofiber was used for burn wound healing, and considerable therapeutic effects were observed.

electrospinning process of nanofibers containing Pcl/Gel/MnO2-NPs was performed. Results of different experiments indicated that the addition of MnO2-NP to the nanofiber structure causes a reduction in the average nanofiber diameter, elasticity, and hydrophilic properties. Also, it causes an increase in the UTS value, water contact angle, porosity, water absorption rate, and degradation rate. The PCL/Gelatin/5%MnO2-NPs nanofiber scaffolds demonstrated the best physical, chemical, and mechanical characteristics for burn wound healing.

The present research showed that a dressing composed of PCL/Gel, 5% MnO2-NPs, and ADSCs can successfully enhance burn wound healing by increasing the collagen synthesis, GAGs content, and wound closure rate, and also reducing the IL1, IL6, and α-SMA levels, and as a result, preventing the scar formation. This wound dressing seems to be a success in regenerative medicine.

Acknowledgment

The authors appreciate the Shahid Beheshti University of Medical Sciences (Tehran, Iran) for the financial support of this study (Grant No. 31451).

Authors' Contribution

Conceptualization: Azin Shahmohammadi, Masoud Soleimani, Farjam Goudarzi.
Formal analysis: Azin Shahmohammadi, Saeed Heidari Keshel, Farjam Goudarzi.
Funding acquisition: Masoud Soleimani.
Investigation: Azin Shahmohammadi, Saeed Heidari Keshel, Farjam Goudarzi.
Methodology: Azin Shahmohammadi, Hadi Samadian, Khodabakhsh Rashidi, Farjam Goudarzi.
Resources: Amir Kiani, Masoud Soleimani.
Supervision: Masoud Soleimani, Farjam Goudarzi.
Writing–original draft: Azin Shahmohammadi, Saeed Heidari Keshel, Farjam Goudarzi.
Writing–review editing: Amir Kiani, Masoud Soleimani.

Competing Interests

The authors have declared no conflict of interest related to this paper.

Ethical Statement

The Ethics Committee of Shahid Beheshti University of Medical Sciences approved all procedures in the present study following NIH (Code: IR.SBMU.AEC.1401.002).

Funding

This experiment was financially supported via the fund from Shahid Beheshti University of Medical Sciences, Tehran, Iran (Grant No. 31451).

Supplementary files

Supplementary file 1 contains Figs. S1-S3.

References

1. Golchin A, Hosseinzadeh S, Jouybar A, Staji M, Soleimani M, Ardeshirylajimi A, Khojasteh A. Wound healing improvement by curcumin-loaded electrospun nanofibers and BFP-MSCs as a bioactive dressing. *Polym Adv Technol* **2020**; 31: 1519-31. https://doi.org/10.1002/pat.4881
2. Kim JW, Kim MJ, Ki CS, Kim HJ, Park YH. Fabrication of bi-layer scaffold of keratin nanofiber and gelatin-methacrylate hydrogel: Implications for skin graft. *Int J Biol Macromol* **2017**; 105: 541-8. https://doi.org/10.1016/j.ijbiomac.2017.07.067
3. Castilla DM, Liu ZJ, Tian R, Li Y, Livingstone AS, Velazquez OC. A novel autologous cell-based therapy to promote diabetic wound healing. *Ann Surg* **2012**; 256: 560-72. https://doi.org/10.1097/SLA.0b013e31826a9064
4. You H-J, Han S-K. Cell Therapy for Wound Healing. *jkms* **2014**; 29: 311-9. https://doi.org/10.3346/jkms.2014.29.3.311
5. Alizadeh E, Zarghami N, Eslaminejad MB, Akbarzadeh A, Barzegar A, Mohammadi SA. The effect of dimethyl sulfoxide on hepatic differentiation of mesenchymal stem cells. *Artificial Cells, Nanomedicine, and Biotechnology* **2016**; 44: 157-64. https://doi.org/10.3109/21691401.2014.928778
6. Rustad KC, Wong VW, Sorkin M, Glotzbach JP, Major MR, Rajadas J, *et al.* Enhancement of mesenchymal stem cell angiogenic capacity and stemness by a biomimetic hydrogel scaffold. *Biomaterials* **2012**; 33: 80-90. https://doi.org/10.1016/j.biomaterials.2011.09.041
7. Yun IS, Jeon YR, Lee WJ, Lee JW, Rah DK, Tark KC, Lew DH. Effect of Human Adipose Derived Stem Cells on Scar Formation and Remodeling in a Pig Model: A Pilot Study. *Dermatol Surg* **2012**; 38: 1678-88. https://doi.org/10.1111/j.1524-4725.2012.02495.x
8. Lam MT, Nauta A, Meyer NP, Wu JC, Longaker MT. Effective Delivery of Stem Cells Using an Extracellular Matrix Patch Results in Increased Cell Survival and Proliferation and Reduced Scarring in Skin Wound Healing. *Tissue Engineering Part A* **2012**; 19: 738-47. https://doi.org/10.1089/ten.tea.2012.0480
9. Chai C, Leong KW. Biomaterials Approach to Expand and Direct Differentiation of Stem Cells. *Mol Ther* **2007**; 15: 467-80. https://doi.org/10.1038/sj.mt.6300084
10. Li W-J, Laurencin CT, Caterson EJ, Tuan RS, Ko FK. Electrospun nanofibrous structure: A novel scaffold for tissue engineering. *J Biomed Mater Res* **2002**; 60: 613-21. https://doi.org/10.1002/jbm.10167
11. Greiner A, Wendorff JH. Electrospinning: A Fascinating Method for the Preparation of Ultrathin Fibers. *Angew Chem Int Ed* **2007**; 46: 5670-703. https://doi.org/10.1002/anie.200604646
12. Nie H, He A, Jia B, Wang F, Jiang Q, Han CC. A novel carrier of radionuclide based on surface modified poly(lactide-co-glycolide) nanofibrous membrane. *Polymer* **2010**; 51: 3344-8. https://doi.org/10.1016/j.polymer.2010.05.014
13. Meng ZX, Zheng W, Li L, Zheng YF. Fabrication and characterization of three-dimensional nanofiber membrance of PCL–MWCNTs by electrospinning. *Materials Science and Engineering: C* **2010**; 30: 1014-21. https://doi.org/10.1016/j.msec.2010.05.003
14. Garg T, Goyal AK. Biomaterial-based scaffolds – current status and future directions. *Expert Opinion on Drug Delivery* **2014**; 11: 767-89. https://doi.org/10.1517/17425247.2014.891014
15. Alvarez-Perez MA, Guarino V, Cirillo V, Ambrosio L. Influence of Gelatin Cues in PCL Electrospun Membranes on Nerve Outgrowth. *Biomacromolecules* **2010**; 11: 2238-46. https://doi.org/10.1021/bm100221h
16. Zhang Y, Ouyang H, Lim CT, Ramakrishna S, Huang Z-M. Electrospinning of gelatin fibers and gelatin/PCL composite fibrous scaffolds. *Journal of Biomedical Materials Research Part B: Applied Biomaterials* **2005**; 72B: 156-65. https://doi.org/10.1002/jbm.b.30128
17. Meng ZX, Zeng QT, Sun ZZ, Xu XX, Wang YS, Zheng W, Zheng YF. Immobilizing natural macromolecule on PLGA electrospun nanofiber with surface entrapment and entrapment-graft techniques. *Colloids Surf B Biointerfaces* **2012**; 94: 44-50. https://doi.org/10.1016/j.colsurfb.2012.01.017
18. Nichol JW, Koshy ST, Bae H, Hwang CM, Yamanlar S,

Khademhosseini A. Cell-laden microengineered gelatin methacrylate hydrogels. *Biomaterials* **2010**; 31: 5536-44. https://doi.org/10.1016/j.biomaterials.2010.03.064
19. Pok S, Myers JD, Madihally SV, Jacot JG. A multilayered scaffold of a chitosan and gelatin hydrogel supported by a PCL core for cardiac tissue engineering. *Acta Biomater* **2013**; 9: 5630-42. https://doi.org/10.1016/j.actbio.2012.10.032
20. Chong EJ, Phan TT, Lim IJ, Zhang YZ, Bay BH, Ramakrishna S, Lim CT. Evaluation of electrospun PCL/gelatin nanofibrous scaffold for wound healing and layered dermal reconstitution. *Acta Biomater* **2007**; 3: 321-30. https://doi.org/10.1016/j.actbio.2007.01.002
21. Yang X, Yang F, Walboomers XF, Bian Z, Fan M, Jansen JA. The performance of dental pulp stem cells on nanofibrous PCL/gelatin/nHA scaffolds. *Journal of Biomedical Materials Research Part A* **2010**; 93A: 247-57. https://doi.org/10.1002/jbm.a.32535
22. Ghasemi-Mobarakeh L, Prabhakaran MP, Morshed M, Nasr-Esfahani M-H, Ramakrishna S. Electrospun poly(ε-caprolactone)/gelatin nanofibrous scaffolds for nerve tissue engineering. *Biomaterials* **2008**; 29: 4532-9. https://doi.org/10.1016/j.biomaterials.2008.08.007
23. Kim MS, Jun I, Shin YM, Jang W, Kim SI, Shin H. The Development of Genipin-Crosslinked Poly(caprolactone) (PCL)/Gelatin Nanofibers for Tissue Engineering Applications. *Macromol Biosci* **2010**; 10: 91-100. https://doi.org/10.1002/mabi.200900168
24. Bang RL, Dashti H. Keloid and hypertrophic scars: trace element alteration. *Nutrition* **1995**; 11: 527-31.
25. Chebassier N, El Houssein O, Viegas I, Dréno B. In vitro induction of matrix metalloproteinase-2 and matrix metalloproteinase-9 expression in keratinocytes by boron and manganese. *Exp Dermatol* **2004**; 13: 484-90. https://doi.org/10.1111/j.0906-6705.2004.00197.x
26. Mahdavi B, Paydarfard S, Zangeneh MM, Goorani S, Seydi N, Zangeneh A. Assessment of antioxidant, cytotoxicity, antibacterial, antifungal, and cutaneous wound healing activities of green synthesized manganese nanoparticles using Ziziphora clinopodioides Lam leaves under in vitro and in vivo condition. *Appl Organomet Chem* **2020**; 34: e5248. https://doi.org/10.1002/aoc.5248
27. Cherian E, Rajan A, Baskar G. Synthesis of manganese dioxide nanoparticles using co-precipitation method and its antimicrobial activity. *International Journal of Modern Science and Technology* **2016**; 1: 17-22.
28. Thangavel P, Ramachandran B, Muthuvijayan V. Fabrication of chitosan/gallic acid 3D microporous scaffold for tissue engineering applications. *Journal of Biomedical Materials Research Part B: Applied Biomaterials* **2016**; 104: 750-60. https://doi.org/10.1002/jbm.b.33603
29. Goudarzi F, Kiani A, Moradi M, Haghshenas B, Hashemnia M, Karami A, Mohammadalipour A. Intraprostatic injection of exosomes isolated from adipose-derived mesenchymal stem cells for the treatment of chronic non-bacterial prostatitis. *J Tissue Eng Regen Med* **2021**; 15: 1144-54. https://doi.org/10.1002/term.3251
30. Dai X, Guan Y, Zhang Z, Xiong Y, Liu C, Li H, Liu B. Comparison of the differentiation abilities of bone marrow-derived mesenchymal stem cells and adipose-derived mesenchymal stem cells toward nucleus pulposus-like cells in three-dimensional culture. *Exp Ther Med* **2021**; 22: 1018. https://doi.org/10.3892/etm.2021.10450
31. Cai EZ, Ang CH, Raju A, Tan KB, Hing ECH, Loo Y, *et al.* Creation of Consistent Burn Wounds: A Rat Model. *Arch Plast Surg* **2014**; 41: 317-24. https://doi.org/10.5999/aps.2014.41.4.317
32. Mirmajidi T, Chogan F, Rezayan AH, Sharifi AM. In vitro and in vivo evaluation of a nanofiber wound dressing loaded with melatonin. *Int J Pharm* **2021**; 596: 120213. https://doi.org/10.1016/j.ijpharm.2021.120213
33. Durmus Z, Kavas H, Baykal A, Toprak MS. A green chemical route for the synthesis of Mn3O4 nanoparticles. *Central European Journal of Chemistry* **2009**; 7: 555-9. https://doi.org/10.2478/s11532-009-0049-4
34. Augustine R, Kalarikkal N, Thomas S. Electrospun PCL membranes incorporated with biosynthesized silver nanoparticles as antibacterial wound dressings. *Appl Nanosc* **2016**; 6: 337-44. https://doi.org/10.1007/s13204-015-0439-1
35. Li H, Wang M, Williams GR, Wu J, Sun X, Lv Y, Zhu L-M. Electrospun gelatin nanofibers loaded with vitamins A and E as antibacterial wound dressing materials. *RSC Adv* **2016**; 6: 50267-77. https://doi.org/10.1039/C6RA05092A
36. DİNcer K, Mpukuta O, ÖZaytekİN İ. Effect of Dynamic Viscosity on Nanofiber Diameters and Electrical Conductivity of Polyacrylonitrile Nanofibers Doped Nano-Cu Particles. *International Journal of Innovative Engineering Applications* **2020**; 4: 1-8. https://doi.org/10.46460/ijiea.707142
37. Hivechi A, Bahrami SH, Siegel RA, B.Milan P, Amoupour M. In vitro and in vivo studies of biaxially electrospun poly(caprolactone)/gelatin nanofibers, reinforced with cellulose nanocrystals, for wound healing applications. *Cellulose* **2020**; 27: 5179-96. https://doi.org/10.1007/s10570-020-03106-9
38. Augustine R, Kalarikkal N, Thomas S. An in vitro method for the determination of microbial barrier property (MBP) of porous polymeric membranes for skin substitute and wound dressing applications. *Tissue Eng Regen Med* **2015**; 12: 12-9. https://doi.org/10.1007/s13770-014-0032-9
39. Jiang P, Lu J, Li K, Chen X, Dan R. Research on hydrophobicity of electrospun Fe3O4/PVDF nanofiber membranes under different preparation conditions. *Fullerenes, Nanotubes and Carbon Nanostructures* **2020**; 28: 381-6. https://doi.org/10.1080/1536383X.2019.1687453
40. Xia J, Zhang H, Yu F, Pei Y, Luo X. Superclear, Porous Cellulose Membranes with Chitosan-Coated Nanofibers for Visualized Cutaneous Wound Healing Dressing. *ACS Appl Mater Interfaces* **2020**; 12: 24370-9. https://doi.org/10.1021/acsami.0c05604
41. Yanilmaz M, Chen C, Zhang X. Fabrication and characterization of SiO2/PVDF composite nanofiber-coated PP nonwoven separators for lithium-ion batteries. *J Polym Sci, Part B: Polym Phys* **2013**; 51: 1719-26. https://doi.org/10.1002/polb.23387
42. Safaee-Ardakani MR, Hatamian-Zarmi A, Sadat SM, Mokhtari-Hosseini ZB, Ebrahimi-Hosseinzadeh B, Kooshki H, Rashidiani J. In situ Preparation of PVA/Schizophyllan-AgNPs Nanofiber as Potential of Wound Healing: Characterization and Cytotoxicity. *Fibers and Polymers* **2019**; 20: 2493-502. https://doi.org/10.1007/s12221-019-9388-8
43. Khorasani MT, Joorabloo A, Moghaddam A, Shamsi H, MansooriMoghadam Z. Incorporation of ZnO nanoparticles into heparinised polyvinyl alcohol/chitosan hydrogels for wound dressing application. *Int J Biol Macromol* **2018**; 114: 1203-15. https://doi.org/10.1016/j.ijbiomac.2018.04.010
44. Doostmohammadi M, Forootanfar H, Shakibaie M, Torkzadeh-Mahani M, Rahimi H-R, Jafari E, *et al.* Bioactive anti-oxidative polycaprolactone/gelatin electrospun nanofibers containing selenium nanoparticles/vitamin E for wound dressing applications. *J Biomater Appl* **2021**; 36: 193-209. https://doi.org/10.1177/08853282211001359
45. Alipour R, Khorshidi A, Shojaei AF, Mashayekhi F, Moghaddam MJM. Skin wound healing acceleration by Ag nanoparticles embedded in PVA/PVP/Pectin/Mafenide acetate composite nanofibers. *Polym Test* **2019**; 79: 106022. https://doi.org/10.1016/j.polymertesting.2019.106022
46. Akturk O, Kismet K, Yasti AC, Kuru S, Duymus ME, Kaya F, *et al.* Wet electrospun silk fibroin/gold nanoparticle 3D matrices for wound healing applications. *RSC Adv* **2016**; 6: 13234-50. https://doi.org/10.1039/C5RA24225H
47. Denzinger M, Held M, Scheffler H, Haag H, Nussler AK, Wendel HP, *et al.* Hemocompatibility of different burn wound dressings. *Wound Repair Regen* **2019**; 27: 470-6. https://doi.org/10.1111/wrr.12739
48. Gounani Z, Pourianejad S, Asadollahi MA, Meyer RL, Rosenholm JM, Arpanaei A. Polycaprolactone-gelatin nanofibers incorporated with dual antibiotic-loaded carboxyl-modified silica nanoparticles. *J Mater Sci* **2020**; 55: 17134-50. https://doi.org/10.1007/s10853-020-05253-7
49. Malemud CJ, Alsberg E. Mesenchymal Stem Cells and

Immunomodulation: An Overview. In: Malemud CJ, E Alsberg, editors. *Mesenchymal Stem Cells and Immunomodulation*. Cham: Springer International Publishing; **2016**. p. 1-5.
50. Ren G, Zhang L, Zhao X, Xu G, Zhang Y, Roberts AI, *et al.* Mesenchymal stem cell-mediated immunosuppression occurs via concerted action of chemokines and nitric oxide. *Cell Stem Cell* **2008**; 2: 141-50. https://doi.org/10.1016/j.stem.2007.11.014
51. Liu S, Jiang L, Li H, Shi H, Luo H, Zhang Y, *et al.* Mesenchymal Stem Cells Prevent Hypertrophic Scar Formation via Inflammatory Regulation when Undergoing Apoptosis. *J Invest Dermatol* **2014**; 134: 2648-57. https://doi.org/10.1038/jid.2014.169
52. Manning CN, Martel C, Sakiyama-Elbert SE, Silva MJ, Shah S, Gelberman RH, Thomopoulos S. Adipose-derived mesenchymal stromal cells modulate tendon fibroblast responses to macrophage-induced inflammation in vitro. *Stem Cell Res Ther* **2015**; 6: 74. https://doi.org/10.1186/s13287-015-0059-4
53. Oryan A, Alemzadeh E, Mohammadi AA. Application of honey as a protective material in maintaining the viability of adipose stem cells in burn wound healing: A histological, molecular and biochemical study. *Tissue Cell* **2019**; 61: 89-97. https://doi.org/10.1016/j.tice.2019.09.007
54. Oryan A, Alemzadeh E, Mohammadi AA, Moshiri A. Healing potential of injectable Aloe vera hydrogel loaded by adipose-derived stem cell in skin tissue-engineering in a rat burn wound model. *Cell Tissue Res* **2019**; 377: 215-27. https://doi.org/10.1007/s00441-019-03015-9
55. Jang H-J, Kim Y-m, Yoo B-Y, Seo Y-K. Wound-healing effects of human dermal components with gelatin dressing. *J Biomater Appl* **2017**; 32: 716-24. https://doi.org/10.1177/0885328217741758
56. Kumar V, Abbas AK, Aster JC. *Robbins and Cotran Pathologic Basis of Disease, Professional Edition E-Book*. Elsevier Health Sciences; **2014**.
57. Hamra NF, Putra A, Tjipta A, Amalina ND, Nasihun T. Hypoxia Mesenchymal Stem Cells Accelerate Wound Closure Improvement by Controlling α-smooth Muscle actin Expression in the Full-thickness Animal Model. *Open Access Macedonian Journal of Medical Sciences* **2021**; 9: 35-41. https://doi.org/10.3889/oamjms.2021.5537